Available online at www.sciencedirect.com
SCIENCE DIRECT®
Thermochimica Acta 427 (2005) 117–128
thermochimica acta
www.elsevier.com/locate/tca

Crystallization kinetics and nucleation activity of filler in polypropylene/surface-treated SiO_2 nanocomposites

George Z. Papageorgiou, Dimitris S. Achilias, Dimitris N. Bikiaris, George P. Karayannidis*

Laboratory of Organic Chemical Technology, Department of Chemistry, Aristotle University of Thessaloniki, GR-54124, Thessaloniki, Macedonia, Greece

Received 14 May 2004; received in revised form 31 August 2004; accepted 7 September 2004
Available online 14 October 2004

Abstract

Isothermal and non-isothermal crystallization kinetics of polypropylene (PP)/surface-treated SiO_2 nanocomposites were extensively studied. Analysis of the isothermal crystallization showed that the phenomenon is characterized by faster rates as the amount of silica is increased. In the case of non-isothermal crystallization, it was found that the Ozawa analysis was rather inapplicable for the nanocomposites. In contrast, the modified Avrami method, as well as the method proposed by Mo was applied giving satisfactory results. The effective energy barrier for non-isothermal crystallization was estimated as a function of the relative degree of crystallinity using the isoconversional analysis of calorimetric data. This was found to vary with the degree of conversion, as well as with the presence of filler. Finally, the nucleation activity of the silica nanoparticles on the polymer matrix was explored and it was proved that when the content of filler exceeds 7.5 wt.% the nucleation is not drastically improved.

Keywords: Crystallization kinetics; Nucleation activity; Polypropylene; Nanocomposites

1. Introduction

The synthesis of new polymeric materials involves high cost therefore research is directed towards modifying current polymers to achieve inexpensive materials with tailored structures and suitable for targeted applications. The use of additives in polymer matrices is a common practice. It usually aims at material reinforcement, enhanced crystallization rates and plasticizing for easier processing. Recently, there has been much research on creating organic/inorganic composites by adding nanoparticles to the polymer matrix [1], resulting thus in materials having greatly improved mechanical and rheological properties [2].

Isotactic polypropylene (i-PP) has become the most interesting commodity thermoplastic, due to its higher isotacticity, enhanced mechanical properties, narrow molecular weight distribution and increased clarity. Therefore, its worldwide production grew up very fast during the last years and there is a tendency to replace some of the traditional polymers in many of their applications. Thermal and mechanical properties of this polymer can be significantly improved using fillers that will act as artificial nucleating agents [3]. Nanoparticles are new classes of fillers, which due to their higher surface area may enhance further the crystallization rate of semicrystalline polymers. SiO_2 nanoparticles are used for effective reinforcement of synthetic rubbers [4], as well as to enhance notch toughness and tensile performance improvement of polypropylene [5–7]. However, different and some times contradictory results have been mentioned about the effect of SiO_2 nanoparticles on crystallization rate of semicrystalline polymers. Rong et al. [6] reported that SiO_2 exhibits some nucleation effect on the crystallization rate of PP matrix though the addition of the nanoparticles does not greatly influence the whole crystalline features of PP. In polyamide 6, unmodified silica nanoparticles increase the crystallization rate of the matrix while modified ones degrease it [8]. In contrast, it was reported that pretreated SiO_2 nanoparticles slightly increased

* Corresponding author. Tel.: +30 2310 997814; fax: +30 2310 997769.
E-mail address: karayan@chem.auth.gr (G.P. Karayannidis).

0040-6031/$ – see front matter © 2004 Elsevier B.V. All rights reserved.
doi:10.1016/j.tca.2004.09.001

the non-isothermal crystallization rates of nylon 6 [9]. In case of larger SiO_2 particle size (5–25 μm) than the nanoscale, it was found that crystallization of polytetrafluoroethylene decreases slightly with the addition of different SiO_2 content [10].

Furthermore, the final polymeric material properties are dependent on the morphology generated during their processing. In this stage, the filler in polymeric-based composite materials may act as a nucleating agent and affect thus the crystallization behavior. So, the knowledge of the parameters affecting crystallization is crucial for the optimization of the processing conditions and the properties of the end product. Research on the polymer crystallization process can be carried out under isothermal or non-isothermal conditions [11]. Analysis of the overall crystallization rate under isothermal conditions is generally accomplished with the use of the so-called Avrami equation [12–17], which is valid at least for the early stages of the process. However, non-isothermal crystallization of polymers is quite difficult to be modelled. Some authors tried to model the non-isothermal process, assuming it can be approximated by a sequence of infinitesimally small isothermal stages, so that it can be described by models based on modifications of the Avrami equation [18–26]. Recently, the non-isothermal crystallization kinetics of several polymer nanocomposites have been studied [27–33]. In this context, although the crystallization kinetics of plain PP have been extensively examined [11], few works dealing with the crystallization kinetics of its nanocomposite have been published [27,33–35].

In this work, the crystallization kinetics of new i-PP nanocomposites containing fumed silica at various amounts, from 1 to 10 wt.%, was studied under both isothermal and non-isothermal conditions. For this purpose various PP/SiO_2 nanocomposites samples were prepared and the effect of SiO_2 content on the crystallization rate of PP was examined. The spherulitic growth rate was used to obtain data on the specific surface free energies for the plain PP and all nanocomposites. Moreover, the kinetic parameters of the Avrami and Ozawa equations were obtained, along with the combined Avrami–Ozawa method. The nucleation activity of the nanoparticles on the polymer matrix was explored. Finally, the effective energy barrier of non-isothermal crystallization was calculated as a function of the relative degree of crystallinity using an isoconversional approach.

2. Experimental

2.1. Materials

Isotactic polypropylene was supplied from BASELL polyolefines with a melt flow index (MFI) 12 g/10 min at 190 °C. The hydrophobic fumed silica (SiO_2) nanoparticles used were supplied from Degussa AG (Hanau, Germany) under the trade name AEROSIL® R974. It was produced by treating hydrophilic fumed silica nanoparticles with dimethyldichlorosilane, and had a specific surface area 170 m^2/g and average primary particle size 12 nm.

2.2. Nanocomposites preparation

Nanocomposites containing 1, 2.5, 5, 7.5 and 10 wt.% SiO_2 nanoparticles were prepared by melt mixing on a Brabender (model DSC Φ25/32D) twin screw corotating extruder with L/D 32 (D25 mm). Along the screw there were different screw elements in order to induce polymer melting and nanoparticle fine dispersion in the polymer melt. Prior to the melt processing, silica nanoparticles were dried for 24 h at 105 °C. After compounding the material was extruded to produce cylindrical extrudates. These were immersed immediately in a cold-water bath (20 °C) and pelletized with an adjustable rotating knife, located after water bath, into 5 mm length.

2.3. Differential scanning calorimetry measurements

Crystallizations of the PP nanocomposites were performed in a Perkin-Elmer Pyris 1 differential scanning calorimeter (DSC). Samples of 5 ± 0.01 mg were used. Isothermal crystallization tests were performed at 125, 127.5, 130, and 132.5 °C. The samples were initially melted at 200 °C for 5 min in order to erase all previous thermal history. The temperature selected to begin the thermal treatment was quite higher than the measured melting point of all composites (around 162 °C), although not very high in order to avoid any possible thermal degradation of the polymer chains. Subsequently, the specimens were cooled at a rate of 200 °C/min to a temperature 20 °C above the crystallization temperature (T_c) and finally at a rate of 40 °C/min to T_c, so that equilibrium of the instrument was achieved. The samples were held at T_c until no change in the heat flow was recorded in the heat flow versus time plot. From the enthalpy evolved during crystallization the kinetics of crystallization was evaluated.

For non-isothermal crystallizations, samples were cooled at various cooling rates. Crystallizations were performed at cooling rates 2.5, 5, 10, and 20 °C/min. The crystallinity of the samples was determined from the heat of crystallization. Fast cooling lead to slightly lower crystallinity.

2.4. Morphological examination

Scanning electron microscopy (SEM) was carried out using a JEOL JMS-840A scanning microscope equipped with an energy-dispersive X-ray (EDX) Oxford ISIS 300 microanalytical system. For this purpose fractured surfaces as well as thin films were used. From these films the Si elemental composition of each nanocomposite sample was determined. The operating conditions were: accelerating voltage 20 kV, probe current 45 nA and counting time 60 s, with ZAF correction being provided on-line. All the studied surfaces were coated with carbon black to avoid charging under the electron beam.

Transmission electron microscopy (TEM) examination was performed in ultra thin sections of nanocomposites by using a JEOL 100 SX microscope.

3. Results and discussion

3.1. Microscopical analysis

In Fig. 1, the silicon elemental analysis at the surface of the nanocomposites films is presented. The density of the white spots is indicative of the amount of the silica particles in the surface of the specimens. In these SEM microphotographs it is obvious that the silica fed in the extruder during compounding, was incorporated into the polymer matrix. However, the SEM cannot provide more information regarding to the microstructure and the dissemination of these particles inside the PP matrix. For this reason the nanocomposites were examined with TEM (Fig. 2). From the TEM microphotographs it was realized that a large amount of silica nanoparticles formed aggregates. Of course the size of these aggregates depends on the silica content and increases as the content of silica increases. In nanocomposites containing 10 wt.% of SiO_2 the aggregates size is up to 500 nm (Fig. 2). This behavior is characteristic of fumed silica and it is attributed to the powerful interaction of the surface hydroxyl groups [3]. For this reason, fumed silica can be found only in aggregates, which form clusters and seems that it is very difficult to break down during melt mixing even when high shear rates are employed as in the extruders.

3.2. Isothermal crystallization kinetics

Crystallization of polymer melts is usually accompanied by significant heat release, which can be measured by differential scanning calorimetry (DSC). Based on the assumption that the evolution of crystallinity is linearly proportional to the evolution of heat released during the crystallization, the relative degree of crystallinity, $X(t)$, can be obtained according to the following equation:

$$X(t) = \frac{\int_0^t (\mathrm{d}H_c/\mathrm{d}t)\mathrm{d}t}{\int_0^\infty (\mathrm{d}H_c/\mathrm{d}t)\mathrm{d}t} \quad (1)$$

where $\mathrm{d}H_c$ denotes the measured enthalpy of crystallization during an infinitesimal time interval $\mathrm{d}t$. The limits t and ∞ are used to denote the elapsed time during the course of crystallization and at the end of the crystallization process, respectively.

Isothermal crystallization of PP and the PP/SiO_2 samples was performed at various temperatures from 125 to 132.5 °C. Fig. 3 shows the DSC traces for isothermal crystallization of the PP/7.5 wt.% SiO_2 nanocomposite. As the supercooling, i.e. the difference between the melting and crystallization temperature, decreases, the crystallization rate gets slower

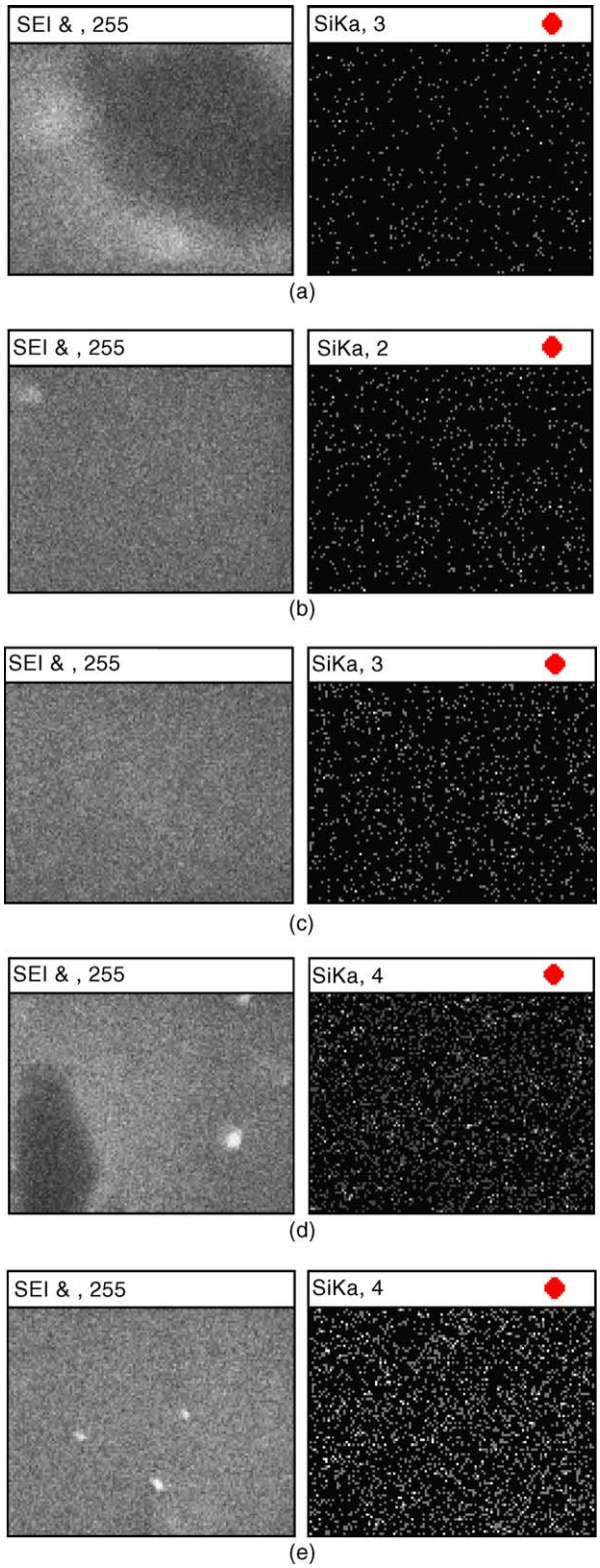

Fig. 1. SEM-EDX microanalysis of silica in PP/surface-treated SiO_2 nanocomposites (a) 1.0 wt.%, (b) 2.5 wt.%, (c) 5.0 wt.%, (d) 7.5 wt.% and (e) 10 wt.%.

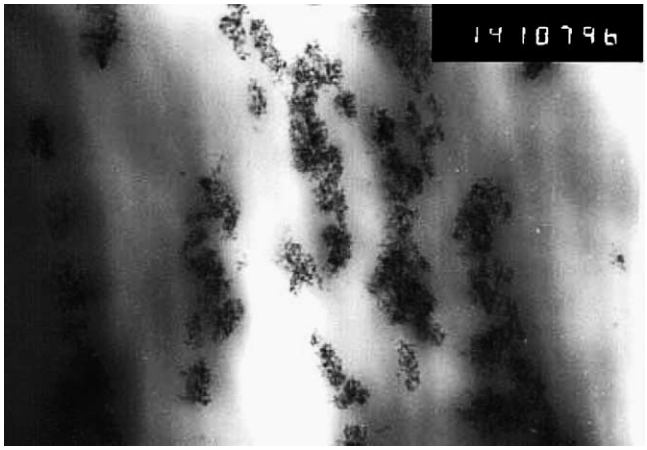

Fig. 2. TEM microphotograph of PP/surface-treated SiO_2 containing 10 wt.% silica nanoparticles.

and the exothermal peak becomes broader. Thus, the time to reach the peak increases.

The application of different macrokinetic models to the isothermal crystallization kinetics of various polymers has been recently investigated by Supaphol et al. [36,37]. For the analysis of the isothermal crystallization, the most common approach is the so-called Avrami method [12–17]. Accordingly, the relative degree of crystallinity, $X(t)$, is related to the crystallization time, t, according to:

$$X(t) = 1 - \exp(-kt^n) \quad \text{or} \quad X(t) = 1 - \exp[-(Kt)^n] \quad (2)$$

where n is the Avrami exponent which is a function of the nucleation process and k is the growth function, which is dependent on nucleation and crystal growth. Since the units of k are a function of n, Eq. (2) can be written in the composite—Avrami form using K instead of k (where $k = K^n$) [36,37]. Avrami equation in the simple form represents unimpeded spherical crystal growth [12–14]. However, the sample does not reach complete crystallization as required for the

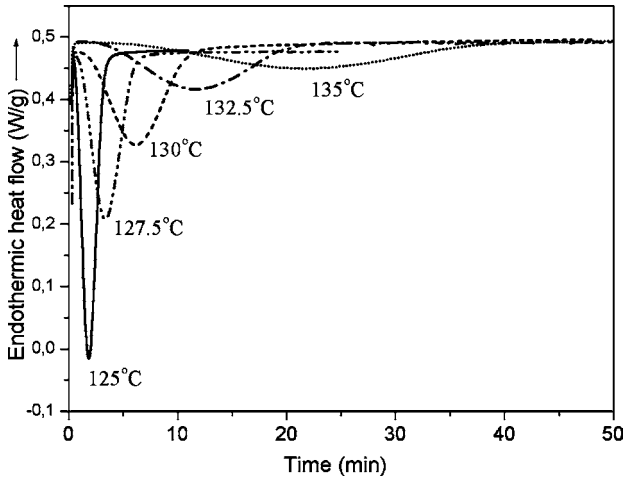

Fig. 3. DSC thermograms of isothermal crystallization for the PP/7.5 wt.% SiO_2 nanocomposite at various temperatures.

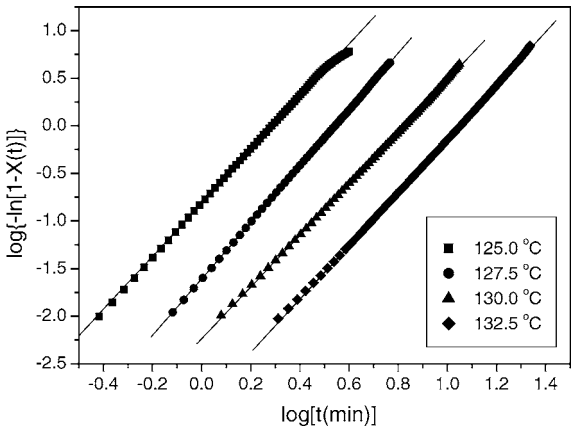

Fig. 4. Avrami plots of $\log[-\ln(1 - X(t))]$ vs. $\log[t]$ for isothermal crystallization of the PP/10 wt.% SiO_2 nanocomposite.

model. To continue the analysis one assumes that complete crystallization is reached. The values of n, k and K, can be calculated from fitting to experimental data using the double logarithmic form of Eq. (2):

$$\log\{-\ln[1 - X(t)]\} = \log k + n \log t \quad (3)$$

Eq. (3) is thus used to fit the experimental data and compare crystallization behaviors of pure PP and the nanocomposites. Plots of $\log\{-\ln[1-X(t)]\}$ versus $\log t$ were constructed and for the isothermal crystallization of the PP/10 wt.% SiO_2 nanocomposite are shown in Fig. 4.

In these plots an initial linear part is observed, which was used for the estimation of the parameters n and k. The deviation, which is observed after this first linear part in the Avrami plots, is often attributed to secondary crystallization. From the slope and the intersection of the Avrami plots, values of n and k, respectively, were calculated and the results are summarized in Table 1. In the same table, the values of K calculated from the respective values of n and k, are included. It is known that the value of n strongly depends on both the mechanism of nucleation and the morphology of crystal growth, and that ideally n would be an integer [12–17]. The n values found in the case of PP nanocomposites were in the vicinity of 2.7, for the crystallization temperatures from 125 to 132.5 °C and they should possibly be related with three-dimensional growth.

Using the n and k values thus obtained, the crystallization half time, $t_{1/2}$, can be calculated from Eq. (4) and their values are presented in Table 1:

$$t_{1/2} = \left(\frac{\ln 2}{k}\right)^{1/n} \quad (4)$$

For a given specimen, the crystallization half time, $t_{1/2}$, increases following the increase in the crystallization temperature, while the inverse effect was observed for the growth function, k. Furthermore, for a given crystallization temperature as the amount of SiO_2 nanoparticles increases, $t_{1/2}$ is reduced while k and K were increased for contents greater than

Table 1
Results of the Avrami analysis for isothermal crystallization of PP and PP/SiO_2 nanocomposites

Samples	T_c (°C)	n	k (min^{-n})	K (min^{-1})	$t_{1/2}$ (min)
PP	125.0	2.6	0.064	0.342	2.53
	127.5	2.5	0.020	0.204	4.21
	130.0	2.5	0.003	0.099	8.74
	132.5	2.6	0.001	0.053	16.5
PP/nano-SiO_2 (1% by weight)	125.0	2.7	0.060	0.355	2.46
	127.5	2.7	0.015	0.212	4.11
	130.0	2.7	0.003	0.119	8.16
	132.5	2.7	0.001	0.059	15.5
PP/nano-SiO_2 (2.5% by weight)	125.0	2.7	0.061	0.360	2.43
	127.5	2.7	0.015	0.216	4.04
	130.0	2.7	0.003	0.117	7.42
	132.5	2.7	0.001	0.063	14.1
PP/nano-SiO_2 (5% by weight)	125.0	2.6	0.102	0.419	2.07
	127.5	2.7	0.022	0.244	3.58
	130.0	2.7	0.006	0.145	6.01
	132.5	2.7	0.001	0.074	11.5
PP/nano-SiO_2 (7.5% by weight)	125.0	2.7	0.105	0.429	2.03
	127.5	2.7	0.027	0.265	3.29
	130.0	2.8	0.008	0.171	5.10
	132.5	2.7	0.001	0.088	9.99
PP/nano-SiO_2 (10% by weight)	125.0	2.8	0.154	0.512	1.71
	127.5	3.0	0.025	0.286	3.09
	130.0	2.7	0.010	0.181	4.84
	132.5	2.8	0.001	0.096	9.01

5 wt.% This verifies that the crystallization rates increase as the nanoparticle content is increased.

3.2.1. Spherulitic growth rate

It has been suggested that the kinetic data of isothermal polymer crystallization can be analyzed using the spherulitic growth rate in the context of the Lauritzen–Hoffman secondary nucleation theory [38,39]. Accordingly, the growth rate G is given as a function of the crystallization temperature, T_c by the following bi-exponential equation:

$$G = G_0 \exp\left[-\frac{U^*}{R(T_c - T_\infty)}\right] \exp\left[-\frac{K_g}{T_c\,\Delta T}\right] \quad (5)$$

where G_0 is the pre-exponential factor, the first exponential term contains the contribution of diffusion process to the growth rate, while the second exponential term is the contribution of the nucleation process; $U^*$and T_∞ are the Vogel-Fulcher-Tamman-Hesse (VFTH) parameters describing the transport of polymer segments across the liquid/crystal interphase, K_g is a nucleation constant and ΔT denotes the undercooling ($\Delta T = T_m^0 - T_c$). The universal values used for the VFTH parameters are $U^* = 1500$ cal/mol (6280 J/mol) and $T_\infty = (T_g - 30)$ K [38,39]. In this study the T_g value of PP used was 270 K [40] and the equilibrium melting temperature, T_m^0 was set equal to 212.1 °C. This value was found by Marand and coworkers [41] using the nonlinear Hoffman-Weeks extrapolation. For a secondary or heterogeneous nucleation, K_g can be calculated from:

$$K_g = \frac{4\sigma\sigma_e b_0 T_m^0}{\Delta h_f \rho_c k_B} \quad (6)$$

where σ, σ_e are the side surface (lateral) and fold surface (end) free energies which measure the work required to create a new surface, b_0 is the single layer thickness taken as 6.26×10^{-10} m assuming (1 1 0) growth front [41], $\Delta h_f \rho_c = \Delta H_f = 1.93 \times 10^8$ J/m^3 is the enthalpy of melting [42,43] and k_B is the Boltzmann constant ($k_B = 1.38 \times 10^{-23}$ J/K). The value of 4 was used since the crystallization was assumed to take place in regime III according to Marand et al. [41]. The nucleation parameter, K_g, can be calculated from Eq. (5) using the double logarithmic transformation:

$$\ln(G) + \frac{U^*}{R(T_c - T_\infty)} = \ln(G_0) - \frac{K_g}{T_c(\Delta T)} \quad (7)$$

If the left-hand-side of Eq. (7) is plotted against $1/(T_c\Delta T)$ a straight line must be obtained having a slope equal to K_g. For the growth rate, G, the approximation: $G \approx 1/t_{1/2}$ [44] can be used. In Fig. 5, these plots are shown for the plain PP and all nanocomposites. As it can be seen all data for every composite follow a straight line with a regression coefficient 0.999. The values of each slope with the corresponding 95% confidence interval are: 9.96 ± 0.61, 9.71 ± 0.75, 9.25 ± 0.37, 8.80 ± 0.55, 8.34 ± 1.14 and 8.16 ± 0.75 for the plain PP and the nanocomposites with 1.0, 2.5, 5.0, 7.5 and 10 wt.% SiO_2, respectively. The K_g values thus obtained are

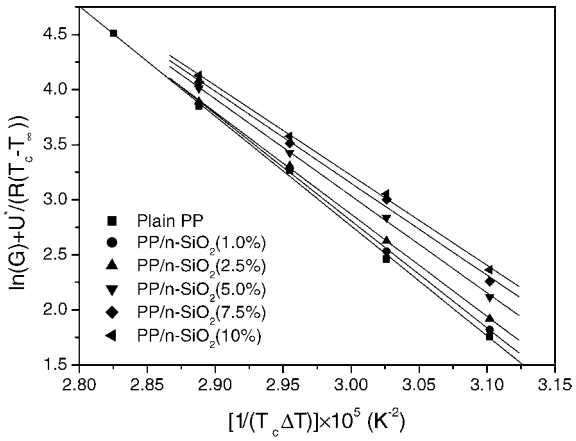

Fig. 5. Lauritzen–Hofmann type plots for isothermal crystallization of all the PP/SiO_2 nanocomposites.

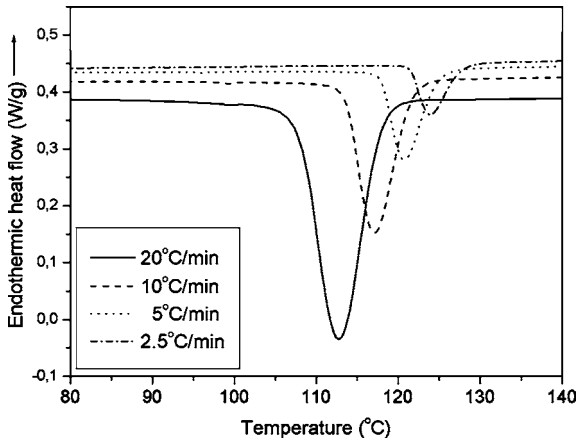

Fig. 7. DSC thermograms of non-isothermal crystallization for the PP/7.5 wt.% SiO_2 nanocomposite at various cooling rates.

plotted with respect to the silica content in Fig. 6. There is a clear tendency for K_g to decrease as the amount of the filler is increased. This decrease is almost linear till 7.5 wt.% SiO_2, while for larger amount of nanoparticles the rate of reduction becomes lower. As it is well known a foreign surface reduces frequently the nucleus size needed for crystal growth since the creation of the interface between polymer crystal and substrate may be less hindered than the creation of the corresponding free polymer crystal surface [44]. A heterogeneous nucleation path makes use of a foreign pre-existing surface to reduce the free energy opposing primary nucleation. It is thus verified that the existence of the silica particles reduces the work needed to create a new surface leading to faster crystallization rates.

3.3. Non-isothermal crystallization kinetics

From dynamic crystallization experiments, data for the crystallization exotherms as a function of temperature, dH_c/dT can be obtained, for each cooling rate, as one can see in Fig. 7 for the crystallization on cooling of PP/7.5 wt.% SiO_2 nanocomposite. The crystallization temperature range becomes broader and it shifts to lower temperatures with increasing cooling rate.

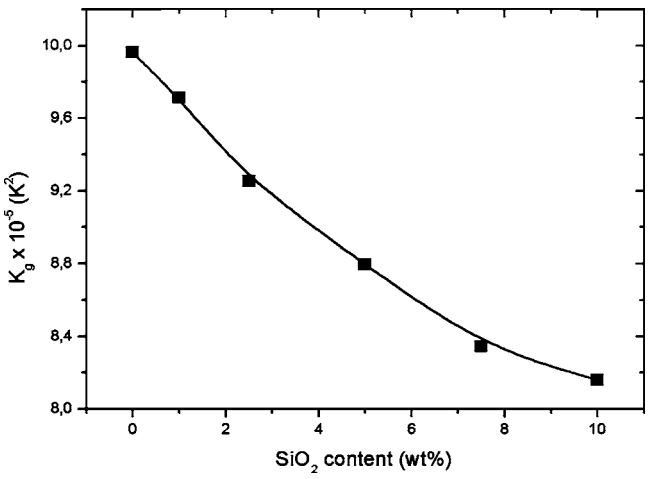

Fig. 6. Variation of the nucleation constant K_g with the silica content, for the PP/SiO_2 nanocomposites.

The relative degree of crystallinity as a function of temperature, $X(T)$, can be formulated as:

$$X(T) = \frac{\int_{T_0}^{T_c} (dH_c/dT)dT}{\int_{T_0}^{T_\infty} (dH_c/dT)dT} \quad (8)$$

where T_0 denotes the initial crystallization temperature and T_c and T_∞ the crystallization temperature at time t and after the completion of the crystallization process, respectively.

Again, the non-isothermal crystallization kinetics of various polymers have been recently investigated by Supaphol et al. [45,46]. The crystallization temperature, T_c, can be converted to crystallization time, t, using the well-known relationship for non-isothermal crystallization processes which is strictly valid when the sample experiences the same thermal history as designed by the DSC furnace [21]:

$$t = \frac{T_0 - T_c}{\alpha} \quad (9)$$

where α is the cooling rate. The transformation from temperature to time is performed using a constant cooling rate [20].

From the DSC thermograms at various cooling rates (2.5, 5, 10 and 20 °C/min), it was found that the crystallization peak temperature, T_p, decreases with increasing cooling rate. For example, the PP crystallization peak temperature for a cooling rate 2.5 °C/min is about 121 °C, while for a cooling rate 20 °C/min it is almost 10 °C lower. A similar behaviour was also observed for the nanocomposites. The respective plots, which show the variation of the peak temperature with cooling rate, for the PP/SiO_2 nanocomposites are shown in Fig. 8. In these plots it is also obvious that the peak temperature at a given cooling rate increases with increasing silica content, and this means that crystallization rates increase with silica content.

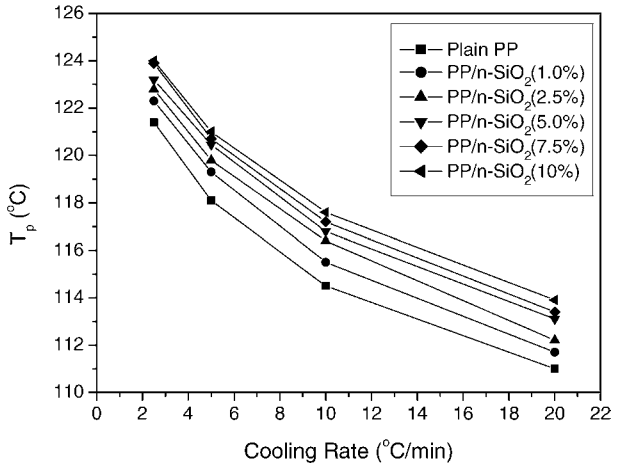

Fig. 8. Crystallization peak temperature against cooling rate for PP/SiO_2 nanocomposites.

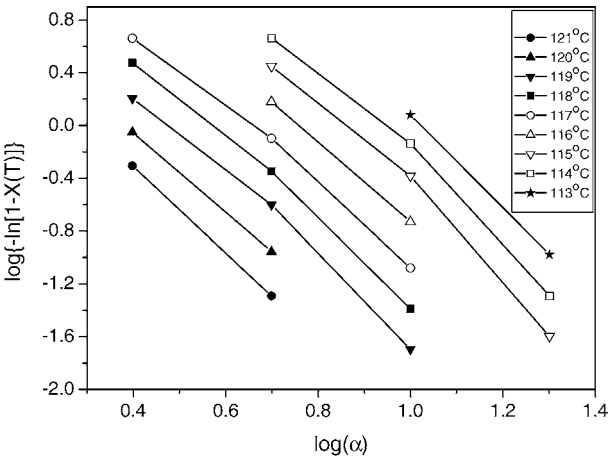

Fig. 9. Ozawa plots of $\log[-\ln(1-X(T))]$ vs. $\log(\alpha)$ for non-isothermal crystallization of the PP/5 wt.% SiO_2 nanocomposite.

In order to quantitatively describe the evolution of crystallinity during non-isothermal crystallization a number of models have been proposed in literature [11,45,46]. In this investigation, the Ozawa [18], the modified-Avrami [21] and the Mo and coworkers [47] analyses were tested.

3.3.1. Ozawa analysis of non-isothermal crystallization

According to Ozawa theory [18], the non-isothermal crystallization process is the result of an infinite number of small isothermal crystallization steps and the degree of conversion at temperature T, $X(T)$, can be calculated as:

$$\ln[1 - X(T)] = -\frac{K^*(T)}{\alpha^m} \tag{10}$$

where m is the Ozawa exponent that depends on the dimension of crystal growth and K^* is the cooling crystallization function. K^* is related to the overall crystallization rate and indicates how fast crystallization occurs. Taking the double-logarithmic form of Eq. (10), it follows:

$$\log\{-\ln[1 - X(T)]\} = \log\ K^*(T) - m\ \log\ \alpha \tag{11}$$

By plotting $\log\{-\ln[1-X(T)\}$ versus $\log\alpha$, a straight line should be obtained and the kinetic parameters, m and K^*, can be achieved from the slope and the intercept, respectively.

Ozawa plots for dynamic crystallization of the PP/SiO_2 nanocomposite containing 5 wt.% nanoparticles are shown in Fig. 9. In the Ozawa plots of the nanocomposites, as well as in plots of PP, increased curvature was observed. In some cases of other polymers like PET, this may be reasonable, because the upper part is related with later stages during which crystallization is retarded, since it takes place in a constrained environment. Ozawa, in his approach, ignored secondary crystallization and the dependence of the fold length on temperature [25]. Lopez and Wilkes [24] claimed that during cooling, secondary crystallization could not take place due to the continuous decrease in temperature. However, the Ozawa analysis is known that it cannot describe adequately crystallization kinetics of polymers such as PE, PEEK and Nylon-11 [11], for which a large part of crystallinity is attributed to secondary crystallization [20]. Thus, in PP/SiO_2 nanocomposites of the present work the Ozawa analysis was thought to be rather inapplicable, and it will be no more discussed.

3.3.2. Avrami analysis of non-isothermal crystallization

According to this model, Eq. (2) can be modified using the transformation (9) in order to describe the crystallization kinetics under non-isothermal conditions:

$$X(t) = 1 - \exp(-Z_t t^n) \tag{12}$$

where Z_t and n denote the growth rate constant and the Avrami exponent, respectively.

Again Z_t and n can be calculated by fitting the experimental data to an equation similar to Eq. (3). In Fig. 10 plots of $\log\{-\ln(1-X)\}$ versus $\log(t)$ are shown for the PP/1 wt.% sample. As it can be seen straight lines are obtained in each cooling rate and from the slope and intercept of each line n

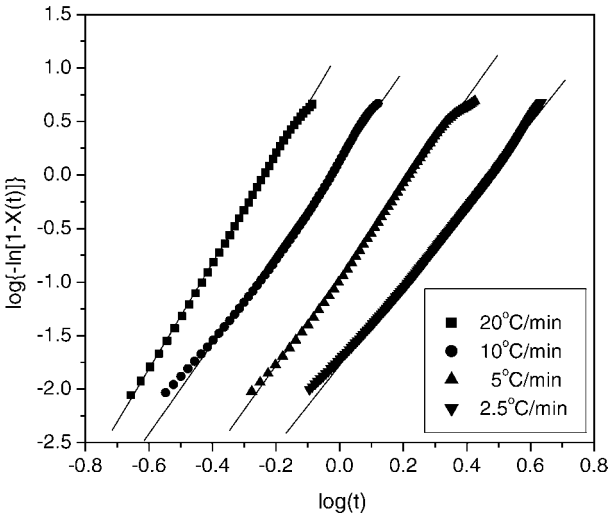

Fig. 10. Avrami plots of $\log[-\ln(1-X(t))]$ vs. $\log[t]$ for non-isothermal crystallization of the PP/1 wt.% SiO_2 nanocomposite.

and log(k) are calculated. Although physical meanings of Z_t and n cannot be related to the non-isothermal case in a simple way, their use provides further insight into the kinetics of non-isothermal crystallization.

Since the rate of non-isothermal crystallization depends on the cooling rate, the crystallization rate constant, Z_t, can be properly corrected to obtain the corresponding rate constant at unit cooling rate, Z_c [21]:

$$\log Z_c = \frac{\log Z_t}{\alpha} \tag{13}$$

Thus, the crystallization half time, $t_{1/2}$, can be calculated from the corrected crystallization constant Z_c using the equation

$$t_{1/2} = \left(\frac{\ln 2}{Z_c}\right)^{1/n} \tag{14}$$

Table 2 summarizes values of the Avrami parameters n, Z_c and of $t_{1/2}$ calculated using Eq. (14) for all the PP nanocomposites at each cooling rate. It should be noted here that the $t_{1/2}$ values thus calculated are different from the ones obtained using the relative degree of crystallinity $X(t)$ data. The crystallization constant, Z_t, increases with increasing cooling rate, while the crystallization half time, $t_{1/2}$, decreases. This is reasonable, since, both Z_t (or Z_c) and $t_{1/2}$ are measures of the crystallization rate, which gets faster with supercooling. Furthermore, as the amount of the SiO_2 nanoparticles is increased, Z_c increases also, for a fixed cooling rate, while $t_{1/2}$ decreases. This proves that the phenomenon has been accelerated because of the presence of the nanoparticles.

The Avrami parameters n and Z_c for PP were found to have very similar values with the corresponding reported by Xu et al. [27]. Values for the exponent decrease as the cooling rate increases, or in other words as the supercooling increases. The Avrami exponents for silica nanoparticle filled PP were less than that for PP at the same cooling rate, indicating that the silica nanoparticles acted as heterogeneous nuclei for the initial nucleation. Therefore the type of nucleation and the geometry of crystal growth of PP changed.

Table 2
Results of the Avrami analysis for non-isothermal crystallization of PP/SiO_2 nanocomposites

Samples	Avrami parameters	Cooling rate (K/min)			
		2.5	5	10	20
PP	n	4.2	4.1	4.2	4.2
	k'	0.15	0.66	1.02	1.15
	$t_{1/2}$	1.44	1.01	0.91	0.89
PP/nano-SiO_2 (1% by weight)	n	3.8	3.7	3.6	3.5
	k'	0.19	0.70	1.03	1.12
	$t_{1/2}$	1.40	0.99	0.90	0.87
PP/nano-SiO_2 (2.5% by weight)	n	4.3	4.0	4.1	3.9
	k'	0.16	0.72	1.10	1.16
	$t_{1/2}$	1.41	0.99	0.89	0.87
PP/nano-SiO_2 (5% by weight)	n	4.2	3.7	3.6	4.0
	k'	0.18	0.79	1.11	1.15
	$t_{1/2}$	1.38	0.97	0.88	0.87
PP/nano-SiO_2 (7.5% by weight)	n	4.2	4.2	4.2	4.0
	k'	0.18	0.79	1.17	1.20
	$t_{1/2}$	1.37	0.97	0.88	0.87
PP/nano-SiO_2 (10% by weight)	n	4.1	3.7	4.1	4.2
	k'	0.20	0.84	1.10	1.30
	$t_{1/2}$	1.36	0.95	0.89	0.87

3.3.3. Mo's analysis

Mo and coworkers [47] proposed a different kinetic model by combining the Ozawa and Avrami equations. As the degree of crystallinity was related to the cooling rate α and the crystallization time t or temperature T the relation between α and t could be defined for a given degree of crystallinity. Consequently, combining Eqs. (3) and (11) derived a new kinetic model for non-isothermal crystallization:

$$\ln Z_t + n \ln t = \ln K^*(T) - m \ln a \tag{15}$$

By rearrangement at a given crystallinity and solving for the cooling rate, Eq. (15) becomes:

$$\ln a = \ln F(T) - b \ln t \tag{16}$$

where $F(T) = [K^*(T)/Z_t]^{1/m}$, refers to the value of cooling rate chosen at unit crystallization time, when the system has a certain degree of crystallinity, b is the ratio of the Avrami exponent to Ozawa exponents, i.e. $b = n/m$. According to Eq. (16) at a given degree of crystallinity the plot of $\ln \alpha$ against $\ln t$ will give a straight line with an intercept of $\ln F(T)$ and a slope of $-b$. As it is shown in Fig. 11, plotting $\ln a$ against $\ln t$, at a given degree of crystallinity, a linear relationship was observed (correlation coefficient $R > 0.998$). The values of $F(T)$ and the slope b are listed in Table 3. The 95% confidence interval on the slope ranges between ± 0.03 and ± 0.08. The $F(T)$ values increased with the relative degree of crystallinity. However, at a certain conversion they remained almost unaffected by the presence of the filler, while b ranged from 1.14 to 1.16 for PP and silica nanoparticle-filled PP composites, which means that the Avrami exponent n is always slightly greater than the Ozawa exponent, m, as it has also been reported in literature [11]. As the amount of the SiO_2 nanoparticles is increased the ratio b is increased, meaning that the presence of the nucleating agent affects in a different way n compared to m. These equations successfully described the non-isothermal crystallization process of PEN and silica nanoparticle-filled PEN [29], as also PP/montmorillonite nanocomposites [27] and Nylon-11 nanocomposites [48]. Non-isothermal crystallization is difficult to be described with a single equation since there are a lot of parameters that have to be taken into account simultaneously. The importance of this method is that it correlates the cooling rate to temperature, time and morphology.

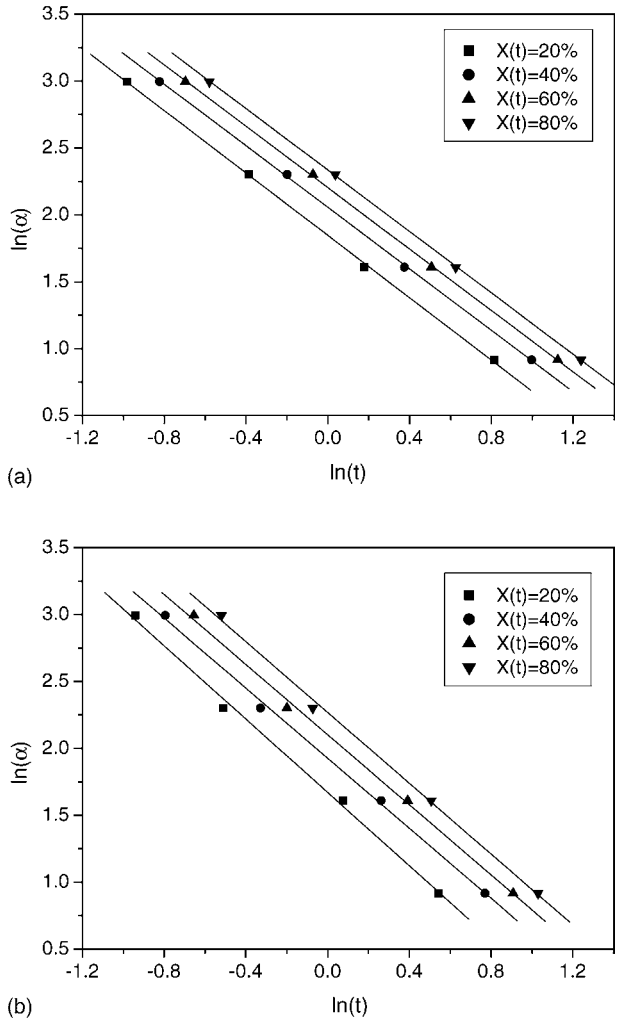

Fig. 11. ln(α) vs. ln(*t*) from the combined Avrami and Ozawa equation for non-isothermal crystallization of (a) plain PP and (b) PP/SiO_2 7.5 wt.%.

3.4. Nucleation activity

Dobreva and Gutzow [49,50] suggested a simple method for calculating the nucleation activity of foreign substrates in polymer melt. This method has been also used for silica nanoparticle-filled PEN [29] and for surface modified talc PP composites [33]. Nucleation activity (φ) is a factor by which the work of three-dimensional nucleation decreases with the addition of a foreign substrate. If the foreign substrate is extremely active, φ approaches 0, while for inert particles, φ approaches 1. The nucleation activity is calculated from the ratio:

$$\varphi = \frac{B^*}{B} \tag{17}$$

where B is a parameter that can be calculated from the following equation:

$$B = \frac{\omega\sigma^3 V_m^2}{3nk_B T_m^0 \Delta S_m^2} \tag{18}$$

Table 3
Values of b and $F(T)$ versus degree of crystallinity based on Mo's treatment for PP and SiO_2 nanoparticle-filled PP composites

Samples	X (%)	b	ln $F(T)$	E (kJ/mol)[a]
PP	20	1.16	1.85	−257
	40	1.15	2.05	
	60	1.15	2.20	
	80	1.15	2.33	
PP/nano-SiO_2 (1% by weight)	20	1.25	1.89	−252
	40	1.24	2.10	
	60	1.23	2.26	
	80	1.21	2.40	
PP/nano-SiO_2 (2.5% by weight)	20	1.15	1.74	−254
	40	1.14	1.95	
	60	1.16	2.10	
	80	1.17	2.23	
PP/nano-SiO_2 (5% by weight)	20	1.13	1.65	−263
	40	1.14	1.86	
	60	1.16	2.02	
	80	1.17	2.17	
PP/nano-SiO_2 (7.5% by weight)	20	1.37	1.67	−258
	40	1.31	1.93	
	60	1.31	2.10	
	80	1.31	2.27	
PP/nano-SiO_2 (10% by weight)	20	1.26	1.74	−268
	40	1.31	1.93	
	60	1.25	2.12	
	80	1.26	2.28	

[a] Effective energy barrier calculated using Kissinger's equation.

where ω is a geometric factor, σ is a specific energy, V_m is the molar volume of the crystallizing substance, n is the Avrami exponent, ΔS_m is the entropy of melting and T_m^0 the infinite crystal melting temperature.

Furthermore, B can be experimentally determined from the slope of Eq. (19) obtained by plotting ln(α) versus the inverse squared degree of supercooling $1/\Delta T_p^2$ ($\Delta T_p = T_m - T_p$) [49,50]:

$$\ln \alpha = \text{Constant} - \frac{B}{\Delta T_p^2} \tag{19}$$

The above equation holds for homogeneous nucleation from a melt, near the melting temperature. By using a nucleating agent, Eq. (19) is transformed to the following for heterogeneous nucleation:

$$\ln \alpha = \text{Constant} - \frac{B^*}{\Delta T_p^2} \tag{20}$$

Plots of ln α versus $1/\Delta T_p{}^2$ for the plain PP and all PP/SiO_2 nanocomposites are shown in Fig. 12. As it can be seen straight lines are obtained in every sample (correlation coefficient $R > 0.998$). From the slopes of these lines, the values of B and B^* for the plain PP and the nanocomposites can be calculated, respectively. These values together with their corresponding 95% confidence interval are 0.948 ± 0.125, 0.934 ± 0.027, 0.917 ± 0.069, 0.874 ± 0.106, 0.808 ± 0.122

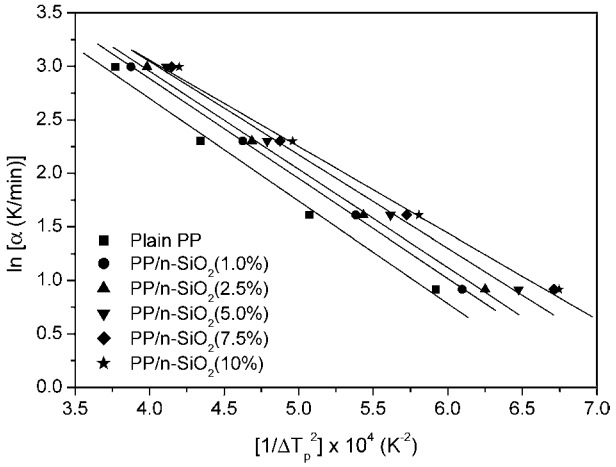

Fig. 12. Plots of $\ln(\alpha)$ vs. $1/\Delta T_p^2$ for PP and all the PP/SiO_2 nanocomposites.

and 0.815 ± 0.085 for the plain PP and the nanocomposites with 1, 2.5, 5, 7.5 and 10 wt.% silica, respectively. Then, the nucleation activity is computed from Eq. (17). The effect of the amount of the nano-SiO_2 on the activity is presented in Fig. 13. From these results, it can be seen that the nucleation effect increased with increasing SiO_2 content, indicating that nano-SiO_2 was acting effectively as a nucleation agent in the PP matrix. However, after a certain amount (i.e., 7.5 wt.%) a plateau is observed meaning that after this amount nucleation is not drastically affected. This might be associated with the increased tendency of the nanoparticles to form aggregates at high filler loads, as it was verified by TEM microphotographs (Fig. 2). It should be noticed that a similar trend was observed for the effect of the amount of SiO_2 nanoparticles on the nucleation constant, K_g calculated using isothermal crystallization data and presented in Fig. 6.

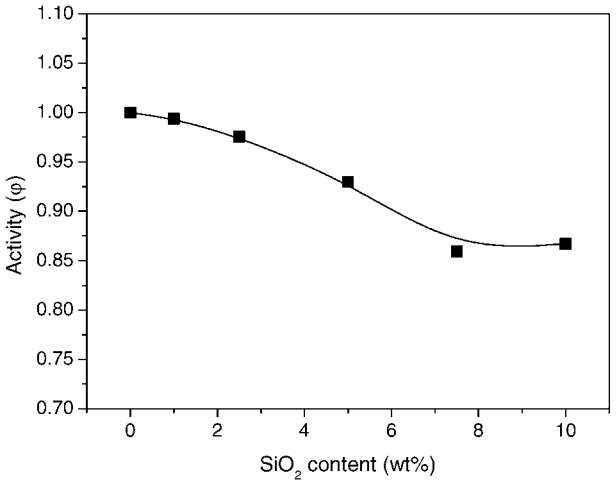

Fig. 13. Variation of nucleation activity (φ) with silica content, for the PP/SiO_2 nanocomposites.

3.5. *Effective energy barrier of non-isothermal crystallization*

Apart from the aforementioned macroscopic kinetic models it is interesting also to evaluate the effective energy barrier, ΔE, for a non-isothermal crystallization process. Considering the variation of the peak temperature with the cooling rate, α, several mathematical procedures have been proposed in literature for the calculation of ΔE [11]. Among them the Kissinger's method has been widely applied in evaluating the overall effective energy barrier:

$$\ln\left(\frac{\alpha}{T_p^2}\right) = \text{Constant} - \frac{\Delta E}{RT_p} \tag{21}$$

Values of the effective energy barrier calculated using the Kissinger's method for all nanocomposites appear in Table 3.

Recently [51], a major concern has been raised for the use of these procedures in obtaining ΔE, since they have been formulated for heating experiments (i.e., positive values of α). Vyazovkin [51] has demonstrated that dropping the negative sign for α is a mathematically invalid procedure that generally makes the Kissinger equation inapplicable to the processes that occur on cooling. Moreover, the use of this invalid procedure may result in erroneous values of the effective energy barrier, ΔE. Furthermore, publication [52] summarizing the results of the ICTAC Kinetic Project has recommended the use of multiple heating rate methods such as isoconversional methods. An isoconversional method can in principle be applied to nonisothermal crystallizations for evaluating the dependence of the effective activation energy on conversion and temperature. Such dependencies have been quite helpful in detecting and elucidating complex kinetics in polymeric systems. The more popular representatives of these methods are the isoconversional methods of Flynn and Wall [53] and Ozawa [54]. According to these methods different effective energy barriers are calculated for every degree of crystallinity, according to the following equation:

$$\ln(\alpha_i) = \text{Constant} - \frac{\Delta E_X}{RT_{X,i}} \tag{22}$$

where ΔE_X is the effective energy barrier at a given degree of crystallinity X, $T_{X,i}$ is the set of temperatures related to a given X at different cooling rates, α_i, and the subscript i refers to every individual cooling rate used.

According to this method, appropriate degrees of crystallinity are selected and the temperature corresponding to each degree for every cooling rate, T_X, is recorded. Then by plotting the logarithmic values of the cooling rate as a function of $1/T_X$ a straight line must appear, with a slope equal to the effective energy barrier. However, according to Vyazovkin and Sbirrazzuoli [55] these methods are likely to be inapplicable to melt crystallization because they require calculation of the logarithm of the heating rate, which is negative for a cooling process and the use of the absolute value may invalidate the calculations. Therefore, the differential isocon-

versional method of Friedman [56] and the advanced integral isoconversional method of Vyazovkin [57] are the most appropriate. In this investigation the method of Friedman was used.

The Friedman equation is expressed as:

$$\ln\left(\frac{\mathrm{d}X}{\mathrm{d}t}\right)_{X,i} = \text{Constant} - \frac{\Delta E_X}{RT_{X,i}} \quad (23)$$

where dX/dt is the instantaneous crystallization rate as a function of time at a given conversion X. According to this method, the $X(t)$ function obtained from the integration of the experimentally measured crystallization rates is initially differentiated with respect to time to obtain the instantaneous crystallization rate, dX/dt. Furthermore, by selecting appropriate degrees of crystallinity (i.e. from 2 to 98%) the values of dX/dt at a specific X are correlated to the corresponding crystallization temperature at this X, i.e. T_X. Then by plotting the left hand side of Eq. (23) with respect to $1/T_X$ a straight line must be obtained with a slope equal to $\Delta E_X/R$. Supaphol et al. [45,46] also used the isoconversional method of Friedman in obtaining results on the effective energy barrier of poly(trimethylene terephthalate).

Plots of ln(dX/dt) versus $1/T_X$ for the PP at different relative crystallinities appear in Fig. 14. As it can be seen, the straight lines obtained are very good, permitting thus the calculation of the effective energy barrier at different degrees of crystallinity. The correlation coefficients obtained were always greater than 0.980.

The dependence of the effective energy barrier on the extent of relative crystallization for the plain PP and the PP/SiO_2 (5 wt.%) and (10 wt.%) nanocomposites is presented in Fig. 15. As it can be seen, ΔE increases with the increase in the relative degree of crystallinity. For both nanocomposites presented the shape of the curve obtained is similar to that observed for PET [58]. However, for plain PP a slight decrease was observed at relative degrees of crystallinity greater than 95%. In all cases ΔE takes great negative values at low extents of conversion that correspond to temperatures closer to the melting point. For the two nanocomposites, the effective energy barrier takes values close to zero only at very high degrees of relative crystallinity (greater than 98%). Furthermore, according to a recent publication [59] the effective energy barrier can be plotted as a function of temperature by taking an average temperature associated with a certain α value (Fig. 16). According to this figure at a given crystallization temperature the effective activation energy increases following the order of plain PP, PP with 5 wt.% nano-SiO_2, PP with 10 wt.% nano-SiO_2. Plots like this can be used in evaluating the Lauritzen–Hoffman parameters [59].

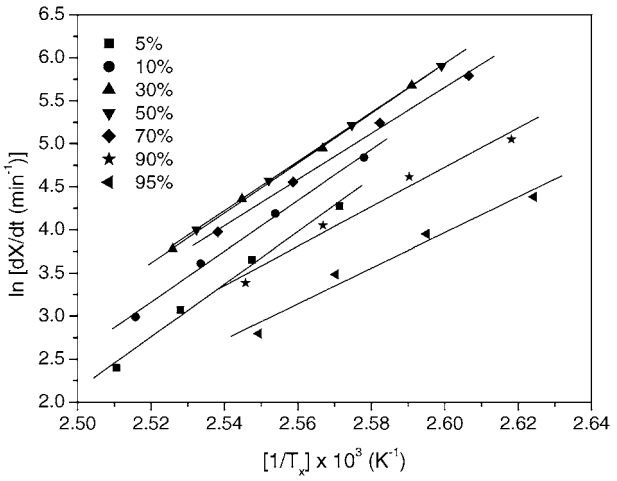

Fig. 14. Friedman-plots of ln(dX/dt) vs. $1/T_X$ for the PP at different relative degrees of crystallinity.

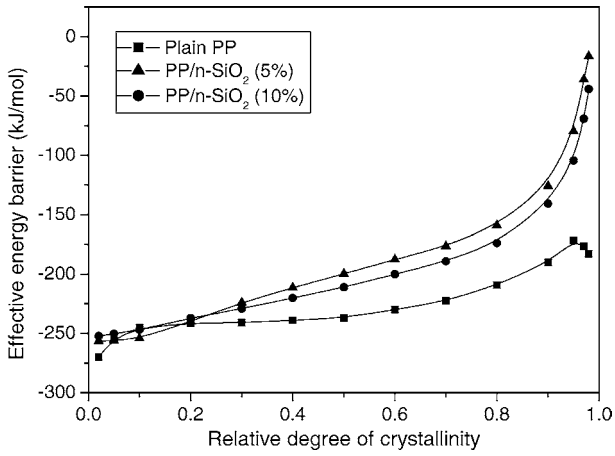

Fig. 15. Dependence of the effective energy barrier on the extent of relative crystallization (isoconversional analysis) for the plain PP and the PP/n-SiO_2 (5 wt.%) and (10 wt.%) nanocomposites.

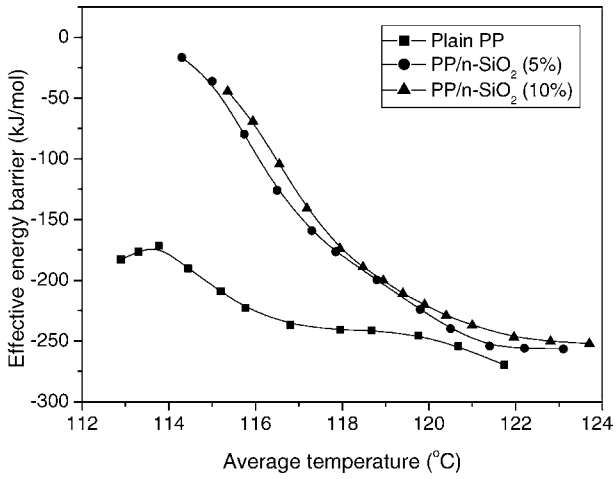

Fig. 16. Dependence of the effective energy barrier on average temperature using the isoconversional analysis for the plain PP and the PP/n-SiO_2 (5 wt.%) and (10 wt.%) nanocomposites.

4. Conclusions

Isothermal crystallization rates of i-PP-fumed silica nanocomposites increased with increasing filler content up

to 7.5 wt.%. In the case of non-isothermal crystallization, it was found that the Ozawa analysis was rather inapplicable for the nanocomposites. In contrast, the modified Avrami method was applied giving satisfactory results, together with the analysis of Mo and coworkers [47]. The effective energy barrier for non-isothermal crystallization was estimated using the isoconversional analysis of calorimetric data. It was found to vary with the degree of conversion. The presence of filler was found to alter the effective energy barrier. Finally, the nucleation activity of the silica nanoparticles was found to increase with the silica amount up to 7.5 wt.%.

Acknowledgements

This work carried out under the financial support of the Greek General Secretariat of Research and Technology under the research program PABE 2000. We would like also to thank professor S. Vyazovkin for his very beneficial and constructive comments on the manuscript.

References

[1] E. Reynaud, T. Jouen, C. Gauthier, G. Vigier, J. Varlet, Polymer 42 (2001) 8759.
[2] J.L. Leblanc, Prog. Polym. Sci. 27 (2002) 627.
[3] S. Sinha Ray, M. Okamoto, Prog. Polym. Sci. 28 (2003) 1539.
[4] Y. Ikeda, S. Kohjiya, Polymer 38 (1997) 4417.
[5] B. Lehmann, K. Friedrich, C.L. Wu, M.Q. Zhang, M.Z. Rong, J. Mater. Sci. Lett. 22 (2003) 1027.
[6] M.Z. Rong, M.Q. Zhang, Y.X. Zheng, H.M. Zeng, R. Walter, K. Friedrich, Polymer 42 (2001) 167.
[7] C.L. Wu, Y.X. Zheng, M.Z. Rong, K. Friedrich, Compos. Sci. Technol. 62 (2002) 1327.
[8] F. Yang, Y. Ou, Z. Yu, J. Appl. Polym. Sci. 69 (1998) 355.
[9] Y. Li, J. Yu, Z.X. Guo, Polym. Int. 52 (2003) 981.
[10] Y.C. Chen, H.C. Lin, Y.D. Lee, J. Polym. Res. 10 (2003) 247.
[11] M.L. Di Lorenzo, C. Silvestre, Prog. Polym. Sci. 24 (1999) 917.
[12] M.J. Avrami, J. Chem. Phys. 7 (1939) 1103.
[13] M.J. Avrami, J. Chem. Phys. 8 (1940) 812.
[14] M.J. Avrami, J. Chem. Phys. 9 (1941) 177.
[15] A.N. Kolmogorov, Izv. Akad. Nauk. SSSR 3 (1937) 355.
[16] W.A. Johnson, R.F. Mehl, Trans. Am. Inst. Mining Metall. Eng. 135 (1939) 416.
[17] U.R. Evans, Trans. Faraday Soc. 41 (1945) 365.
[18] T. Ozawa, Polymer 12 (1971) 150.
[19] K. Nakamura, K. Katayama, T. Amano, J. Appl. Polym. Sci. 17 (1973) 1013.
[20] A. Ziabicki, A. Sakjiewitz, Colloid Polym. Sci. 276 (1998) 680.
[21] A. Jeziorny, Polymer 19 (1978) 1142.
[22] M.C. Tobin, J. Polym. Sci.: Polym. Phys. 12 (1974) 399.
[23] P. Cebe, S.D. Hong, Polymer 27 (1986) 1183.
[24] L.C. Lopez, L.G. Wilkes, Polymer 30 (1989) 882.
[25] M.L. Addonizio, C. Martuscelli, Silvestre, Polymer 28 (1987) 183.
[26] R.M. Patel, J.H. Bheda, J. Spruiell, J. Appl. Polym. Sci. 42 (1991) 1671.
[27] W. Xu, M. Ge, P. He, J. Polym. Sci.: Polym. Phys. 40 (2002) 408.
[28] J. Qian, P. He, J. Mater. Sci. 38 (2003) 2299.
[29] S.H. Kim, S.H. Ahn, T. Hirai, Polymer 44 (2003) 5625.
[30] M.Z. Rong, M.Q. Zhang, Y.X. Zheng, H.M. Zeng, K. Friedrich, Polymer 42 (2001) 3301.
[31] Y. Ou, F. Yang, Z.Z. Yu, J. Polym. Sci.: Polym. Phys. 36 (1998) 789.
[32] X. Liu, Q. Wu, Eur. Polym. J. 38 (2002) 1383.
[33] M. Alonso, J.I. Velasco, J.A. De Saja, Eur. Polym. J. 33 (1997) 255.
[34] W. Zhu, G. Zhang, J. Yu, G. Dai, J. Appl. Polym. Sci. 91 (2004) 431.
[35] P. Guschl, J.U. Otaigbe, J. Appl. Polym. Sci. 90 (2003) 3445.
[36] P. Supaphol, Thermochim. Acta 370 (2001) 37.
[37] N. Dangseeyun, P. Srimoaon, P. Supaphol, M. Nithitanakul, Thermochim. Acta 409 (2004) 63.
[38] J.D. Hoffman, G.T. Davis, J.I. Lauritzen Jr., in: N.B. Hannay (Ed.), Treatise on Solid State Chemistry, vol. 3, Plenum Press, New York, 1976 (Chapter 7).
[39] J.D. Hoffman, R.L. Miller, Polymer 38 (1997) 3151.
[40] Advanced Thermal Analysis System (ATHAS Databank) available in http://web.utk.edu/athas/edu.
[41] J. Xu, S. Srinivas, H. Marand, P. Agarwal, Macromolecules 31 (1998) 8230.
[42] H.S. Bu, S.Z.D. Cheng, B. Wundrlich, Makromol. Chem. Rapid Commun. 9 (1988) 76.
[43] G. Natta, P. Pino, P. Corradini, F. Danusso, E. Mantica, G. Mazzanti, G. Moraglio, J. Am. Chem. Soc. 77 (1952) 1708.
[44] M. Mucha, Z. Krolikowski, J. Therm. Anal. Cal. 74 (2003) 549.
[45] P. Supaphol, N. Dangseeyun, P. Srimoaon, M. Nithitanakul, Thermochim. Acta 406 (2003) 207.
[46] P. Supaphol, N. Dangseeyun, P. Srimoaon, Polym. Test 23 (2004) 175.
[47] T. Liu, Z. Mo, S. Wang, H. Zhang, Polym. Eng. Sci. 37 (1997) 568.
[48] S. Lie, Y. Yu, Y. Cui, H. Zhang, Z. Mo, J. Appl. Polym. Sci. 70 (1998) 2371.
[49] A. Dobreva, I. Gutzow, J. Non-Cryst. Solids 162 (1993) 1.
[50] A. Dobreva, I. Gutzow, J. Non-Cryst. Solids 162 (1993) 13.
[51] S. Vyazovkin, Macromol. Rapid Commun. 23 (2002) 771.
[52] M.E. Brown, M. Maciejewski, S. Vyazovkin, R. Nomen, J. Sempere, A. Burnham, J. Opfermann, R. Strey, H.L. Anderson, A. Kemmler, R. Keuleers, J. Janssens, H.O. Desseyn, C.-R. Li, T.B. Tang, B. Roduit, J. Malek, T. Mitsuhashi, Thermochim. Acta 355 (2000) 125.
[53] J.H. Flynn, L.A. Wall, J. Res. Natl. Bur. Stand. (US) 70A (1966) 487.
[54] T. Ozawa, Bull. Chem. Soc. Jpn. 38 (1965) 1881.
[55] S. Vyazovkin, N. Sbirrazzuoli, J. Phys. Chem. B 107 (2003) 882.
[56] H. Friedman, J. Polym. Sci. Part C 6 (1964) 183.
[57] S. Vyazovkin, J. Comput. Chem. 22 (2001) 178.
[58] S. Vyazovkin, N. Sbirrazzuoli, Macromol. Rapid Commun. 23 (2002) 766.
[59] S. Vyazovkin, N. Sbirrazzuoli, Macromol. Rapid Commun. 25 (2004) 733.